Magnetic-directed closed-loop lead recycling from spent perovskite photocatalysts toward sustainable CO_2 reduction

Jingyi Hou, Jiaying Rong, Jing Feng, Shuo Tao, Qiao Chen*, Ranran Fu, Manqing Xu, Linxing Shi, Yuanyuan Zhang*

School of Science, Jiangsu Ocean University, Lianyungang 222005, People's Republic of China

*** Corresponding authors:**

E-mail address: chenqiao@jou.edu.cn (Q. Chen); zhangyuanyuan@jou.edu.cn (Y. Zhang)

Section S1. Material preparation

CsBr (99.5%), $PbBr_2$ (99.0%), dimethyl sulfoxide (DMSO, 99.3%), isopropanol (IPA, 99.5%), $FeCl_3$(99.0%), $Co(NO_3)_3 \cdot 6H_2O$ (99.0%), NaBr (99.0%), acetonitrile (99%), and tetrabutylammonium hexafluorophosphate (98%) were all purchased from Shanghai Macklin Biochemical Co., Ltd. HNO_3 (99.7%) was purchased from Chengdu Cologne Chemical Co., Ltd. NaOH (96.0%) was obtained from Shanghai Yien Chemical Technology Co., Ltd. Resin was supplied by Kehai Si (Beijing) Technology Co., Ltd.

Section S2. First-principles calculations

First-principles calculations were performed to determine the electronic band structure and partial density of states (PDOS). All calculations employed the generalized gradient approximation (GGA) with the Perdew–Burke–Ernzerhof (PBE) functional for geometry optimization, during which atomic positions and lattice parameters were fully relaxed. The following convergence criteria were applied: an energy tolerance of 5.0×10^{-6} eV per atom, a maximum Hellmann-Feynman force of 0.01 eV/Å, a maximum stress of 0.02 GPa, and a maximum atomic displacement of 5.0×10^{-4} Å.

Section S3. Energy consumption considerations in cost analysis

To evaluate the economic feasibility of recovering $PbBr_2$ from perovskite materials, a detailed cost analysis is performed, with the results summarized in Table S1. The total cost for one recovery using the present closed-loop strategy is ¥2.38, equivalent to 5.34 ¥/g, while the commercial $PbBr_2$ cost is 6.88 ¥/g. In the cost analysis, labor, equipment depreciation and energy inputs associated with the recovery process are taken into consideration, including personnel time for operation and monitoring, as well as electricity consumption for stirring, magnetic separation, and other equipment. Despite these extra expenses being relatively higher than material costs, they are important considerations for assessing overall process economics. Overall, compared with the potential risks associated with lead contamination, the closed-loop strategy of recovering and recycling $PbBr_2$ proves to be both economically favorable and environmentally sustainable.

Table S1. Cost comparisons for R-$PbBr_2$ for one recovery versus C-$PbBr_2$.

Cost component	Price (¥/g or ¥/mL)	Cost (¥)
DMSO	0.16	1.60
NaBr	0.20	0.31
HNO_3	0.01	0.11
NaOH	0.03	0.06
Resin (reusable)	0.12	0.30
Recovered $PbBr_2$	5.34	2.38
Extra expenses		
Energy	0.5 (¥/kw·h)	1.47
Labor	26.67 (¥/d)	4.45
Depreciation	20 (¥/time)	0.67
Commercial $PbBr_2$	6.88	

Section S4. Scalability of magnetic-directed closed-loop recycling strategy

The core processes with magnetic separation, ion exchange, and solvent recovery are all scalable. The resin exhibits high selectivity for Pb^{2+}, significantly reducing pre-treatment requirements. Large-scale operation benefits from economies of scale, while energy consumption can be further reduced through heat integration and continuous processing. High-gradient magnetic separation enables rapid capture of magnetic $CoFe_2O_4$ from large volumes, outperforming batch centrifugation. With appropriate engineering solutions, this process holds strong promise for cost-effective lead recovery at large scales.

Section S5. Preliminary life cycle assessment of magnetic-directed recycling

A preliminary life cycle assessment based on multi-cycle experimental data shows that solvent recovery in the closed-loop system significantly reduces fresh solvent use and hazardous waste generation. Lead recovery efficiency is high, preventing most lead from environmental release. The material circularity indicator for lead reaches a high value, reflecting effective loop closure. Although upstream and downstream impacts are not yet fully covered, the available data indicate clear environmental advantages in resource conservation and pollution prevention. A more comprehensive assessment will be conducted when pilot-scale data become available.

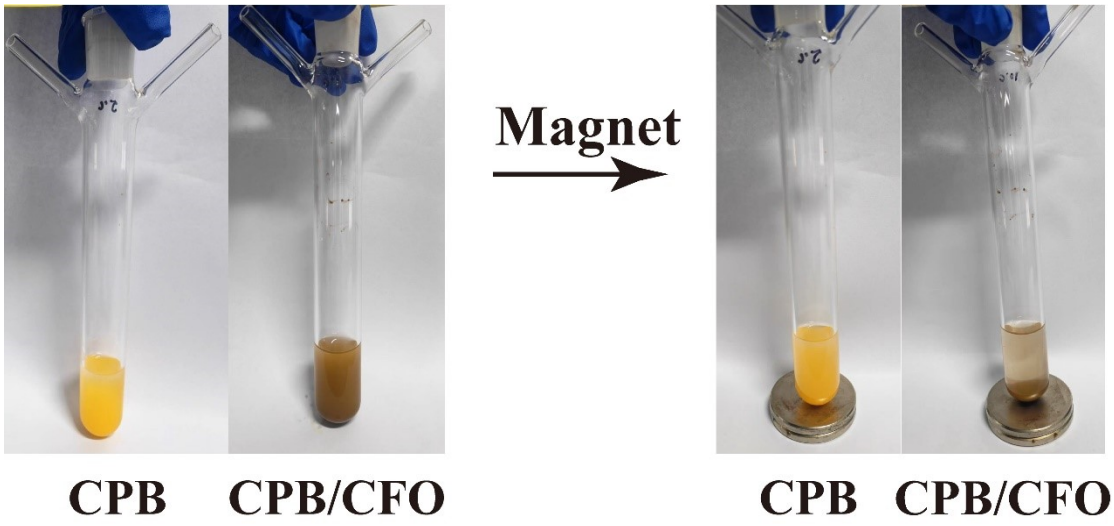

Fig. S1. Photos of dispersed non-magnetic CPB and magnetic CPB/CFO catalyst in reaction quartz tube before and after magnetic separation.

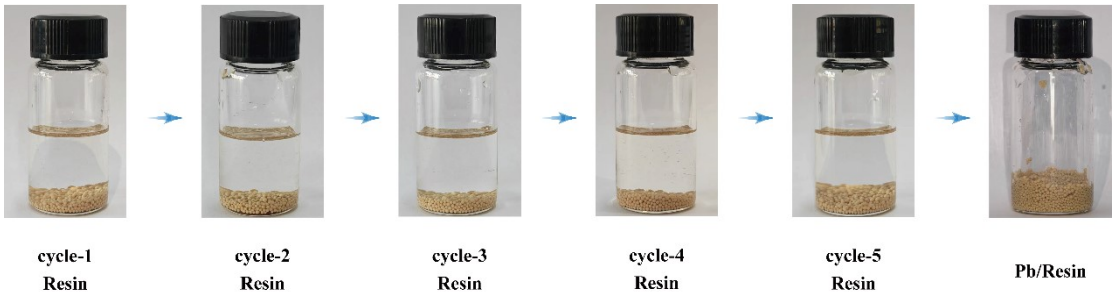

Fig. S2. Photos of repeated resin adsorption and Pb^{2+} richness process.

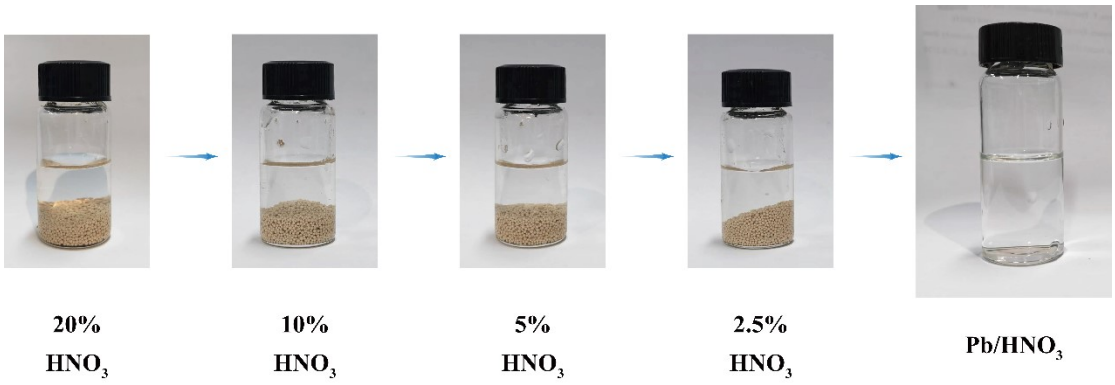

Fig. S3. Photos of elution process for resin by gradient concentration HNO_3 solution.

Fig. S4. Photos of directional precipitation of Pb^{2+} into $Pb(OH)_2$ by pH control.

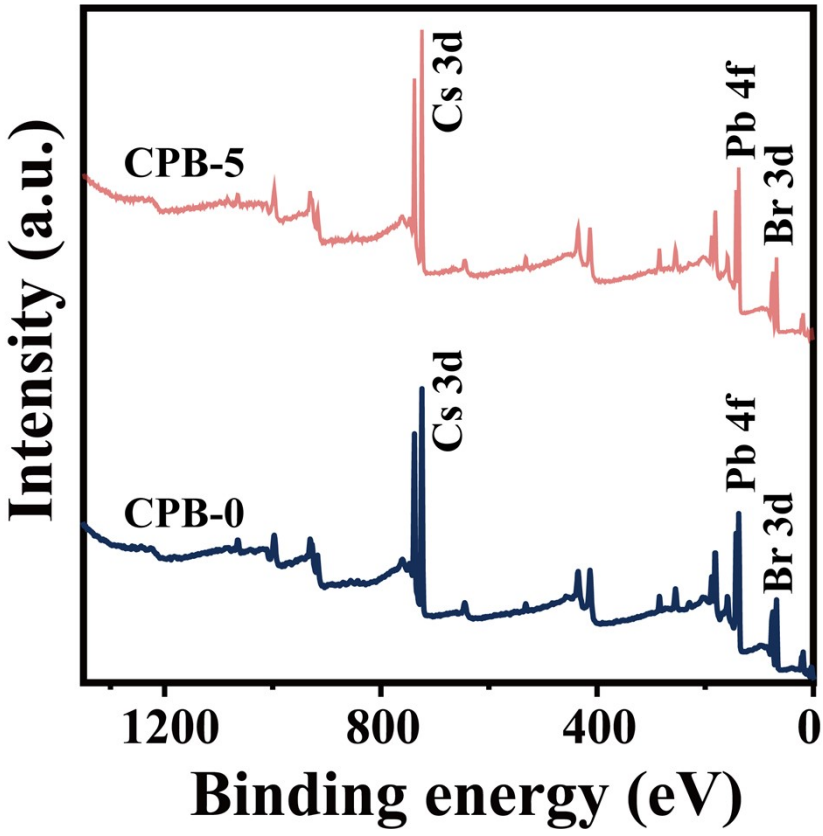

Fig. S5. XPS survey spectra of CPB fabricated using PB-0 and PB-5

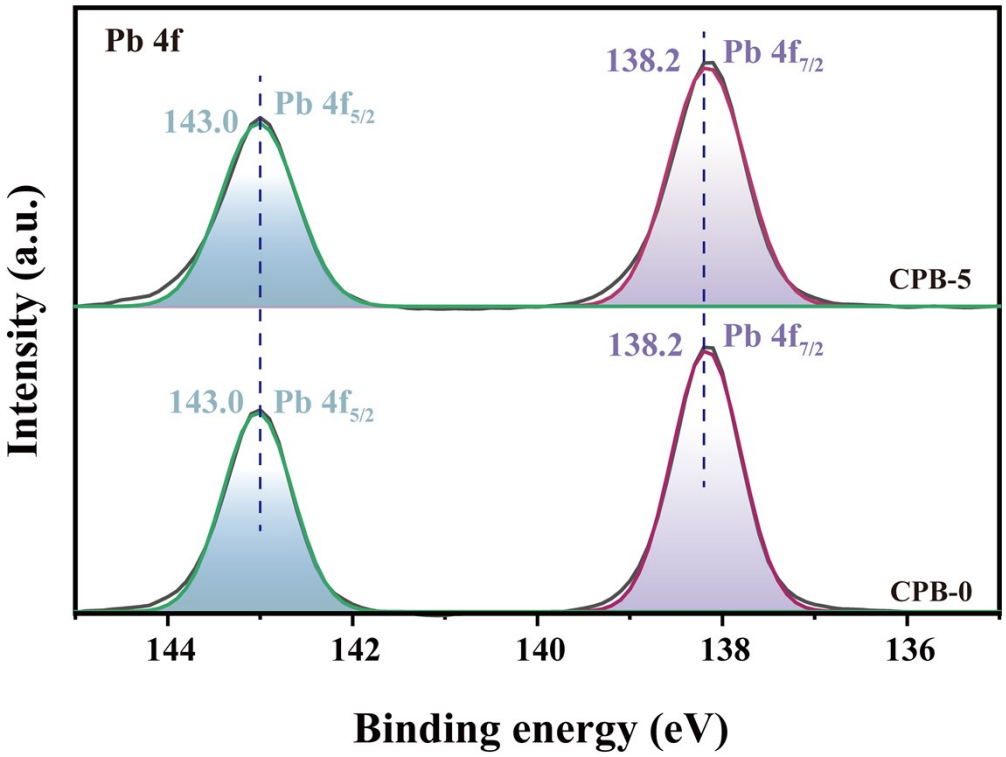

Fig. S6. XPS spectra of Pb 4f peaks for CPB-0 and CPB-5.

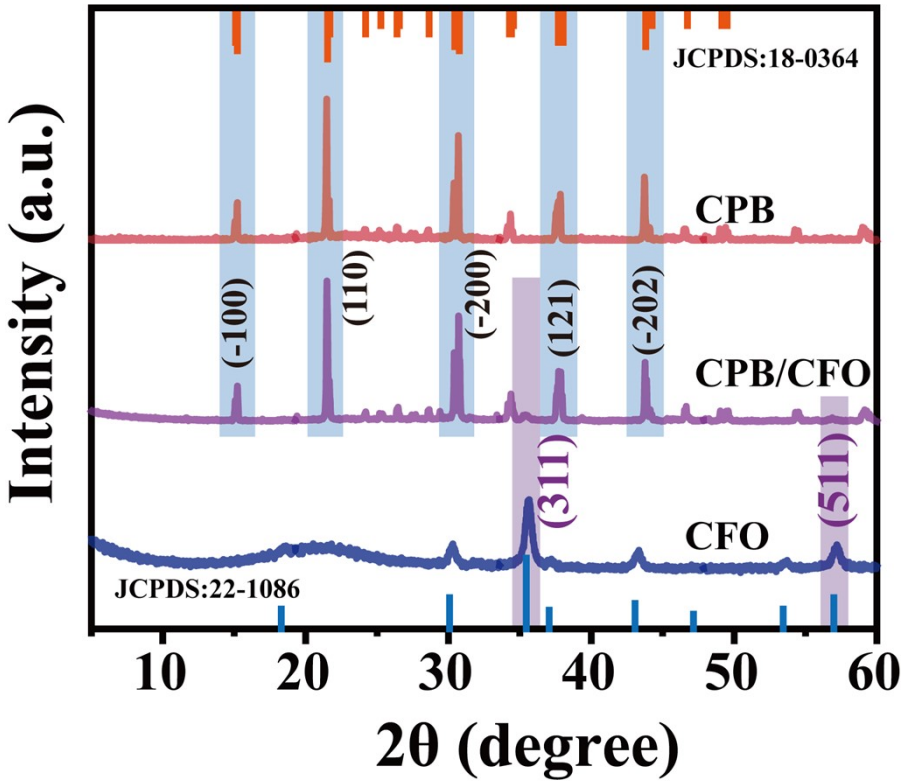

Fig. S7. XRD patterns of CPB, CPB/CFO composite and CFO.

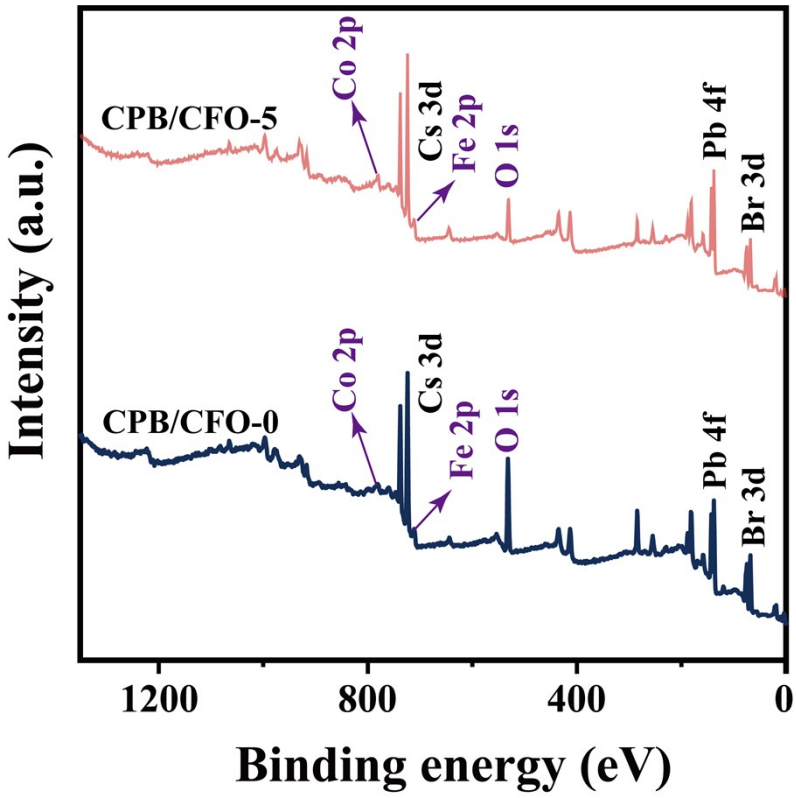

Fig. S8. XPS survey spectra of CPB/CFO constructed by CPB-0 and CPB-5.

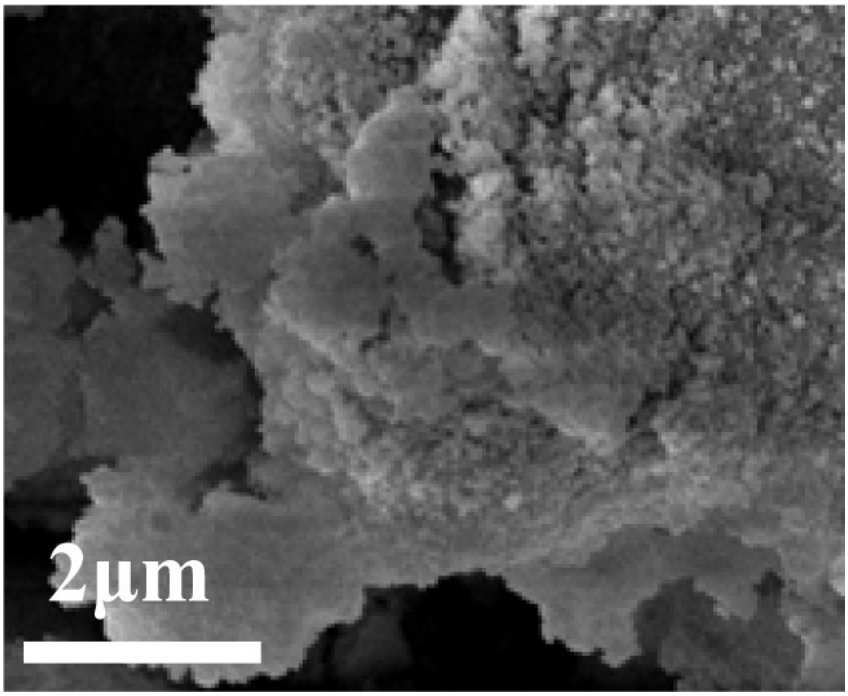

Fig. S9. SEM image of CFO cocatalyst.

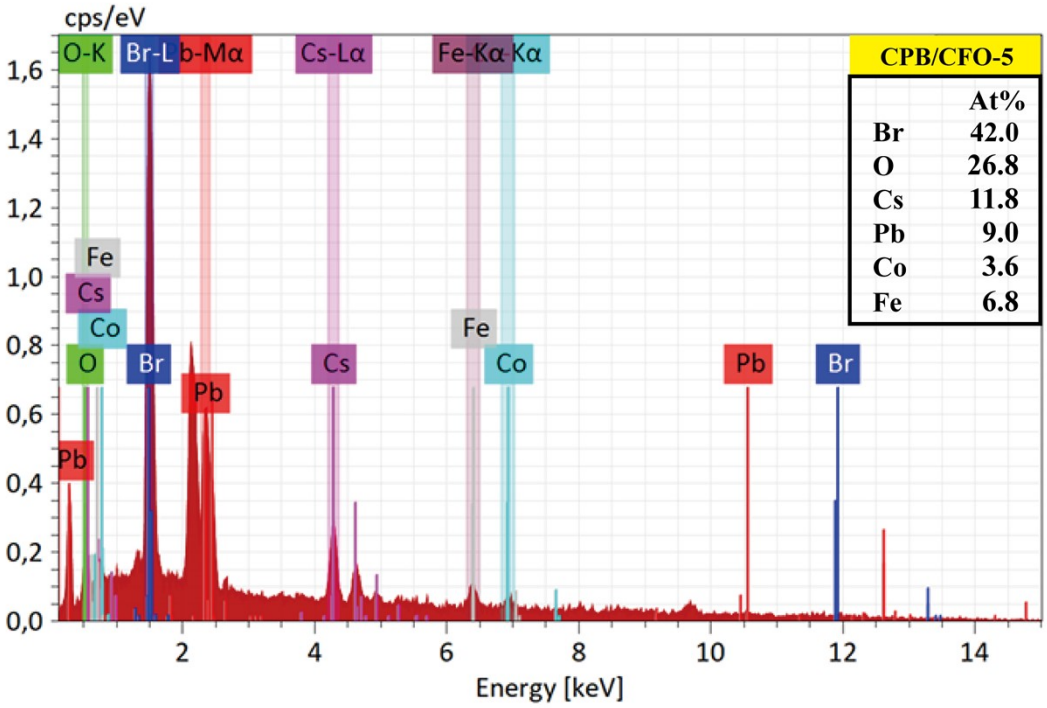

Fig. S10. EDS spectrum and element contents of R-CPB/CFO-5 composite.

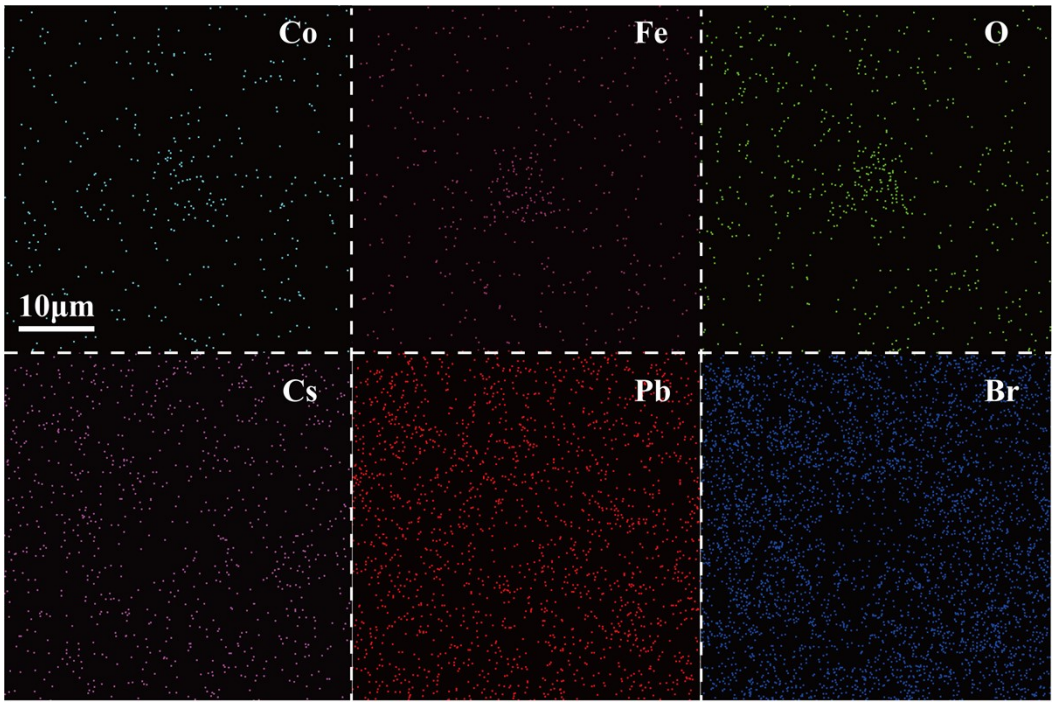

Fig. S11. Elemental mapping of C-CPB/CFO-0 composite.

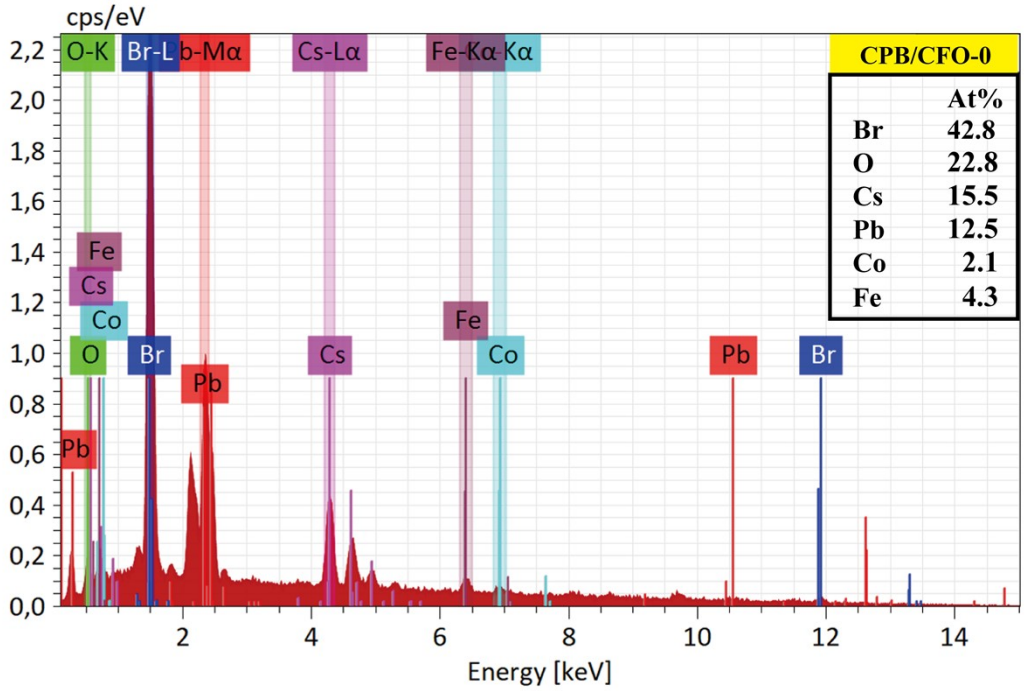

Fig. S12. EDS spectrum and element contents of C-CPB/CFO-0 composite.

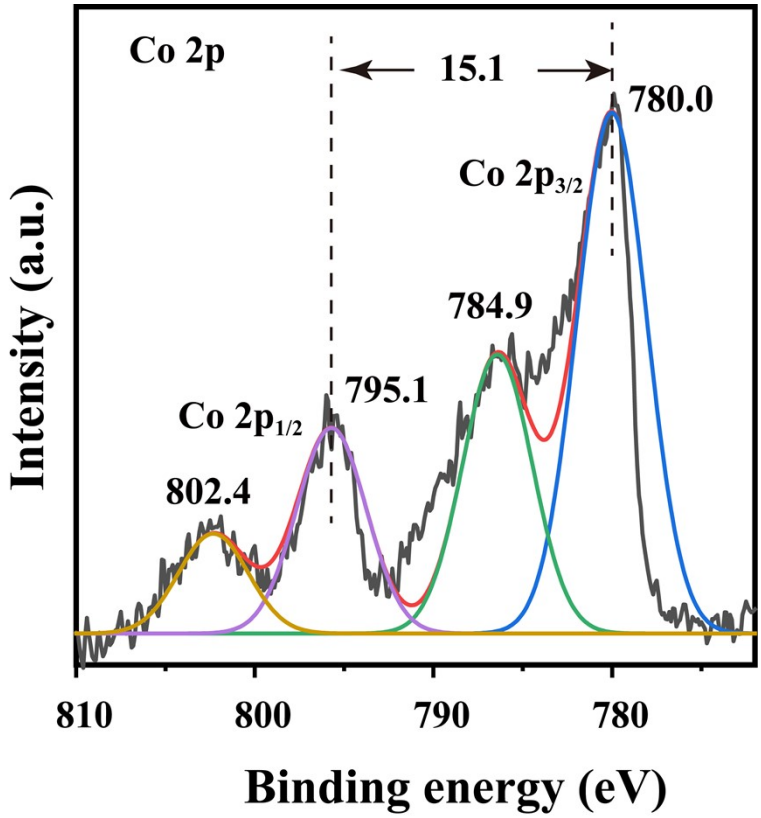

Fig. S13. XPS spectra of Co 2p peaks for CPB/CFO catalyst.

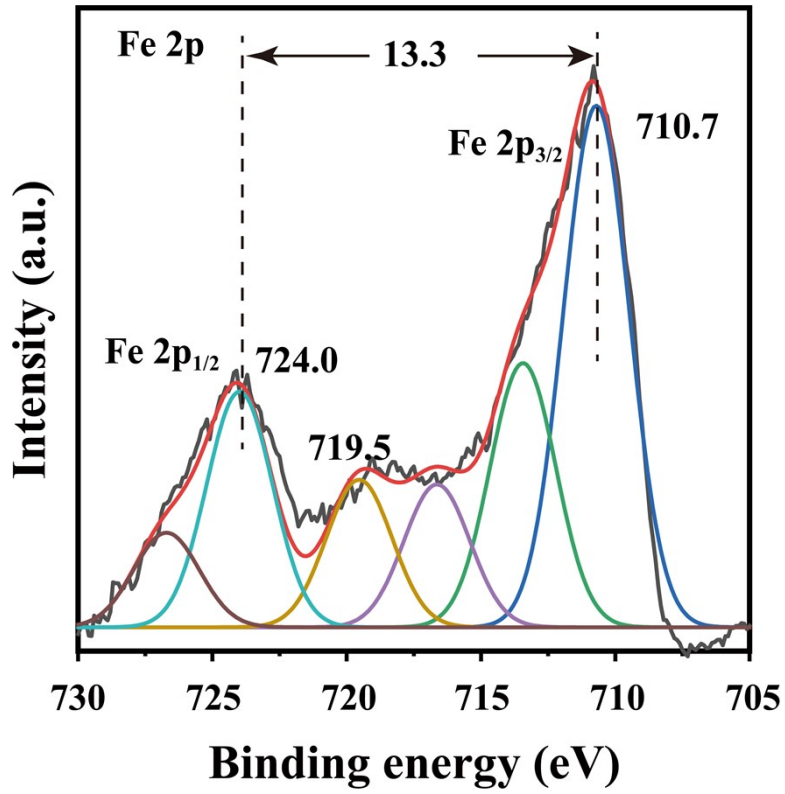

Fig. S14. XPS spectra of Fe 2p peaks for CPB/CFO catalyst.

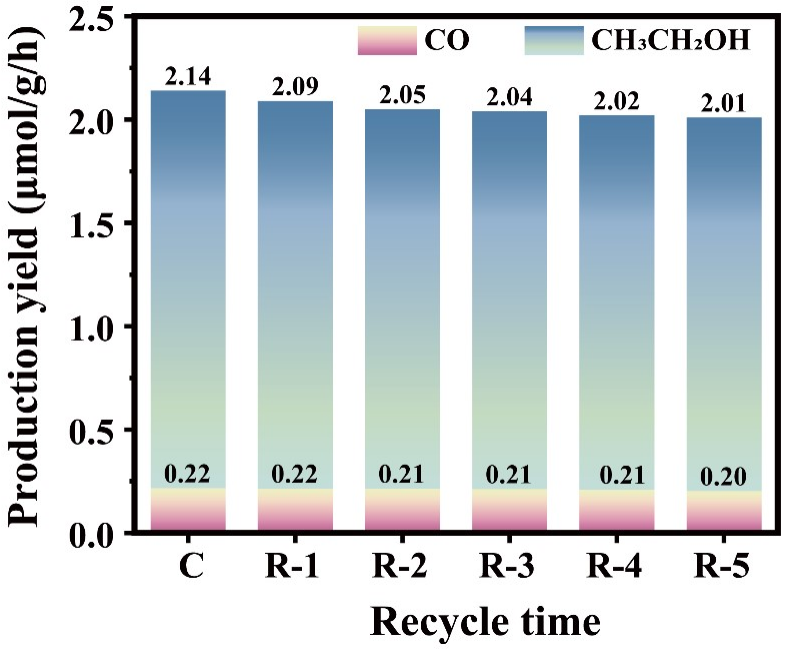

Fig. S15. Product yields of pristine R-CPB catalyst regenerated from different recovery cycles.

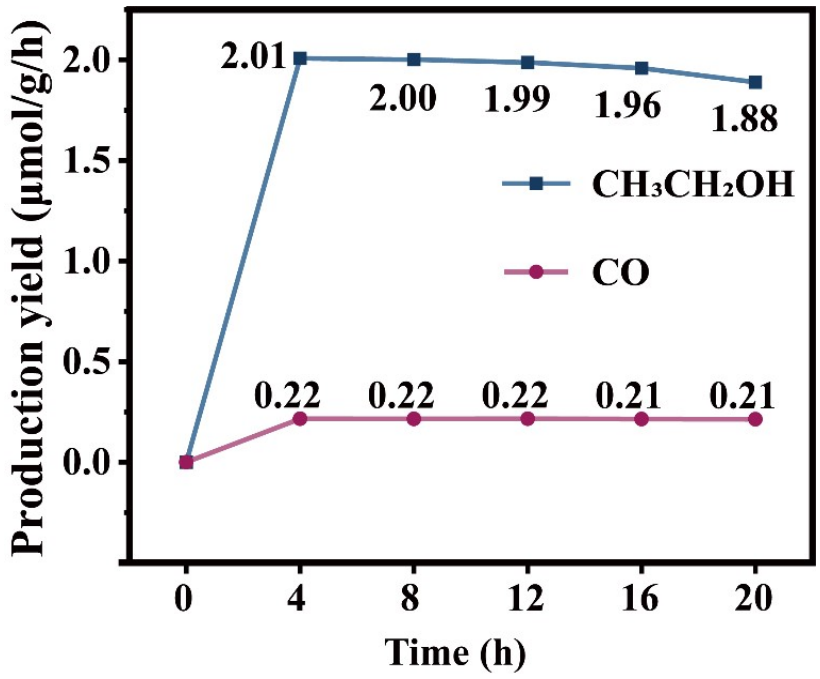

Fig. S16. Cycling stability of the pristine R-CPB over multiple reuse cycles.

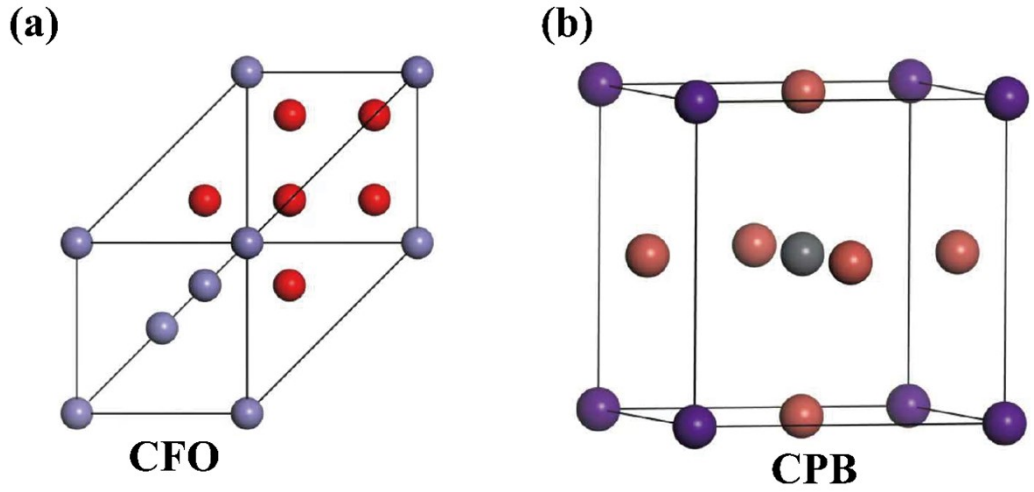

Fig. S17. Crystal structures of (a) CFO and (b) CPB for first-principles calculations.